LUND UNIVERSITY

Sorting cells by size, shape and deformability.

Beech, Jason; Holm, Stefan; Adolfsson, Karl; Tegenfeldt, Jonas

Link to publication

Total number of authors:
4

Lab on a Chip

COMMUNICATION

Sorting cells by size, shape and deformability†

Jason P. Beech,[*a] **Stefan H. Holm,**[a] **Karl Adolfsson**[a] **and Jonas O. Tegenfeldt**[ab]

While size has been widely used as a parameter in cellular separations, in this communication we show how shape and deformability, a mainly untapped source of specificity in preparative and analytical microfluidic devices can be measured and used to separate cells.

Morphology has been used successfully for centuries for classification of species across all kingdoms of life ranging from bacteria to mammals and identification of disease through histological samples. During the past decades there has been an increasing fundamental interest in the connection between the shape of cells, their overall function and the underlying molecular networks. Yet a limited effort has been made to develop fast and efficient ways to sort based on shape. Imaging cytometry is one example; however it is limited by the resolution and speed of the sorting. A small number of microfluidic techniques have been developed recently to address these concerns.[1,2] Deformability of cells is an important clinical indicator of a wide range of medical conditions and is measured in bulk using, for example, ektacytometry.[3] Microfluidic approaches include the laser stretcher,[4] obstacle arrays,[5,6] margination[7] and inertial focussing.[8] None of the above-mentioned high-throughput approaches can be used for detailed high-resolution studies of the mechanical properties of large number of cells. Furthermore, although shape may influence the result in the above devices, with exception for direct imaging, the shape of the deformed particles and the anisotropy of the deformability cannot be discerned in the measurements.

Deterministic lateral displacement[9] (DLD) has been demonstrated to be a powerful mechanism for highly precise continuous sorting based on size. Devices consist of arrays of posts through which particles smaller than a critical radius, R_c, move with the flow and particles larger than the critical radius move along a direction defined by the device. For hard spherical particles, the operation of the device is straightforward, however, biological particles are often soft and non-spherical and their deformability and shape are known to influence the trajectories of the particles in DLD devices.[10–12] In this communication we explore the extent of these relative contributions and present an approach that opens up for sorting and

aDivision of Solid State Physics, nmC@LU, Lund University, PO Box 118, S-221 00 Lund, Sweden. E-mail: jason.beech@ftf.lth.se; Fax: +46 (0)46 222 3637; Tel: +46 (0)46 2222 4956
bDepartment of Physics, University of Gothenburg, Gothenburg, Sweden
† Electronic supplementary information (ESI) available. See DOI: 10.1039/c2lc21083e

characterisation based on targeting them specifically as separation parameters.

We can define an effective size, R_{eff}, for a particle of arbitrary shape and deformability as the radius of a hard spherical particle that would follow an identical trajectory through a DLD device. In our simplified model we consider $2R_{eff}$ as the projected width of a particle along a line, transverse to the overall flow direction, joining the centres of two posts (Fig. 1A). At this decision point the trajectory of the particle is determined by the relation between R_{eff} and R_c. The critical radius, R_c, in turn depends on the geometry of the array in a highly complex way but much of the behaviour can be captured surprisingly well by making the gross simplification of considering R_c also as the projected width of the first flow stream on this same line (Fig. 1A).

Because the effective size of a non-spherical particle depends on its orientation as it passes between two posts, the key to shape sensitive sorting is to control this orientation. One simple way to achieve this is through confinement of the particles: in deep devices non-spherical particles tend to become aligned in the flow between posts such that their smallest dimension defines R_{eff}. Conversely in a shallow device rotation is hindered, which for some particle shapes leads to a larger dimension defining R_{eff}. For example, by confining disc-shaped red blood cells, RBCs, in a device with depth less than the overall diameter, the trajectory of the particles is determined by a combination of their overall diameter and thickness. For sufficiently strong confinement, at a depth of approximately the thickness of the cell, the trajectory is entirely determined by the overall diameter, see Fig. 1D (and ESI† Section 2 for further details). This simple approach can now be used to measure different particle dimensions and to separate particles that would have identical R_{eff} in a deep device.[1]

Due to shear forces from the carrier fluid and normal forces from the stationary posts, a deformable particle will assume an increasingly elongated shape moving through a device as shear forces are increased, which in turn will change the effective radius, R_{eff}. Thus by gradually changing the shear rates and observing the effective sizes of the particles, we essentially perform a stress–strain measurement on the particles from which we can extract information about the mechanical properties of the cells.

All in all this gives us the ability to select the relative contributions of size, shape and deformability to the trajectories of the particles in applications including analysis, concentration, or separation.

We have evaluated our method using RBCs. Not only are the morphologies[13] and deformabilities[14] of RBCs of great clinical interest but because RBCs are both readily available and their shapes
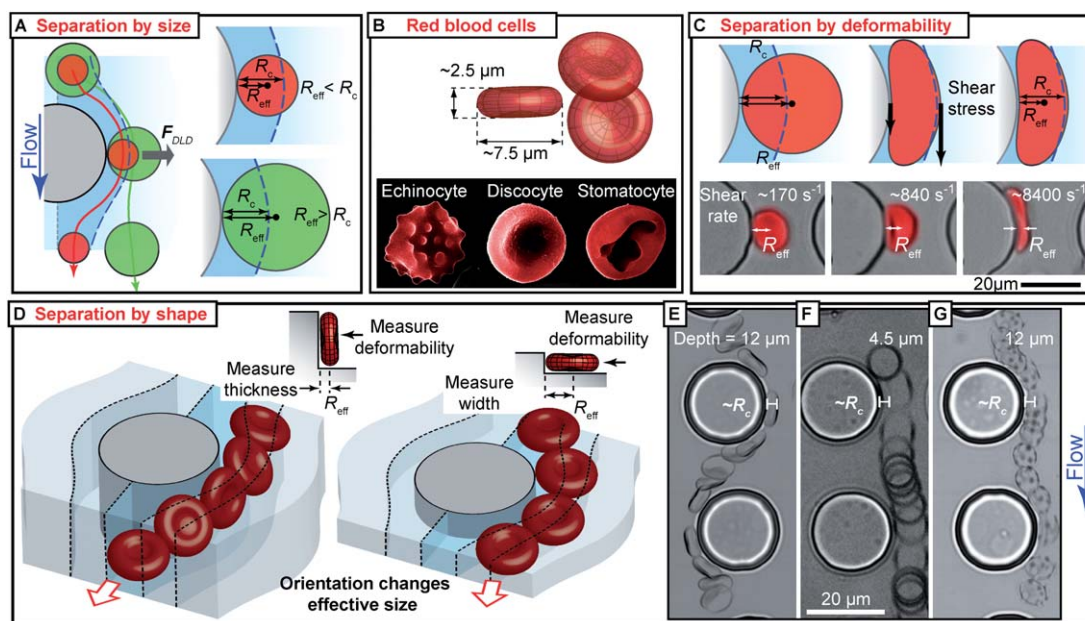
Fig. 1 Mechanisms of separation by DLD. (A) Particles with $R_{eff} < R_c$ follow the flow direction and those with $R_{eff} > R_c$ are displaced at an angle to the flow direction. For hard spheres, R_{eff} is equal to the radius. (B) Red blood cells are normally disc-shaped but they can adopt other shapes when exposed to different chemicals. (C) Shear forces deform particles changing R_{eff}, and measuring the change in R_{eff} as a function of applied shear rate is equivalent to measuring the deformability of the particle. (D) R_{eff} depends on the orientation of the particle. Controlling orientation and measuring R_{eff} gives information about shape. It is also possible to measure deformability in different directions. (E) In a deep device RBCs rotate such that R_{eff} ($<R_c$) is equal to half the thickness. (F) Confinement in a shallow device means that the cell radius defines R_{eff} ($>R_c$). (G) An echinocyte with $R_{eff} > R_c$.

and mechanical properties easily changed[15] they constitute an excellent model system for cells in general provided one keeps in mind that RBCs lack a nucleus and are therefore much simpler than most other cells.

Several models explain RBC shape, the most prominent being the bilayer-couple theory.[15,16] It relies on an asymmetry in composition between the two leaflets of the lipid bilayer forming the cell membrane, which means that the leaflets react differently to perturbations while remaining coupled to one another. If, for example, the area of one leaflet is altered, the resulting strain in the other leaflet will be relieved by bending the bilayer in analogy to the bending of a bimetallic strip upon heating. This bending can have a dramatic effect on both the shape of the cell and on its mechanical properties, and underlies many of the methods that are used to modify RBC morphologies.[14] Osmolarity provides another way to control the shape of a RBC but changes not only the shape of the cell but also the volume. In the current work we use sodium salicylate (SS) and Triton™ X-100 (TX) which modify the relative areas of the inner and outer leaflets, to form echinocytes and stomatocytes respectively without significantly altering cell volume. We used 16 mM SS[17] and 580 ppm TX,[18] which we found to give the most homogeneous and stable populations of RBCs with regard to morphologies, see Fig. 1B.

Experiments are performed in the following way. 1. Blood is drawn from healthy volunteers and prepared strictly adhering to a simple protocol as described in the ESI† Section 1.4 to minimize any variation in the morphology and/or deformability of the cells as a result of the handling of the blood. 2. The RBCs are injected into the device (ESI† Section 1.5) and a series of films are taken at low magnification of the outlet distribution of the cells as the driving pressure is changed across the range 5 to 800 mbar corresponding to wall shear rates (the maximum rate at the surface of the posts) in the range 40 to 6700 s^{-1}

and 100 to 16 400 s^{-1} for the two device depths used (4.27 ± 0.04 μm and 10.84 ± 0.12 μm). To be able to map out the effective size with high resolution our devices are designed and fabricated with R_c ranging from 1.5 to 4.5 μm in 13 steps (see the ESI† Section 1.1–3). Remember, the outlet distribution reflects the effective size of the cells and we can characterize this using polystyrene microspheres of known sizes. 3. Particle tracking software (described in the ESI† Section 1.6) is used to determine the distribution of RBCs at the end of the device. 4. In order to verify the deformation of the cells, high-speed films (100 to 10 000 frames s^{-1}) at high magnification are also taken of cells moving through devices.

In Fig. 1E–G RBCs can be seen moving through a device at low shear rates such that they are not measurably deformed. The rotation of an RBC in a 12 μm deep‡ device results in the smallest possible R_{eff} as is clearly seen in Fig. 1E. In this array R_{eff} is defined by half of the thickness of the cell ~1.25 μm < R_c ~3 μm and the cell is therefore following the flow, which is evidenced by the fact that it crosses the column of posts. In a 4.5 μm deep device‡, shown in Fig. 1F, the RBC is forced to lay flat and R_{eff} is defined instead by the overall radius of the cell ~3.75 μm which is larger than R_c so that the cell moves in the displacement mode. See the ESI† (Section 2) for a graph summarizing the effect of device depth. Fig. 1G shows an echinocyte moving through the 12 μm device‡. Each echinocyte suffers a contraction in its width and a dilation in its thickness relative to the discocytes such that it is almost spherical while R_{eff} is still greater than R_c and the cell is displaced. This is interesting because what would be seen in a blood smear as a decrease in cell size actually leads to an increase in effective size in our device.

Fig. 1C shows images of deformation of RBCs moving through a 4.27 μm deep device at different shear rates acquired with a high-speed camera. As before, at a device depth of 4.27 μm the cells are

constrained to lie in the plane of the device. As the shear rate is increased, the deformation of the cells increases. It can clearly be seen how this deformation leads to a decrease in the width of the particle and therefore of R_{eff} (additional images and movies of RBCs with different morphologies in devices of 4.27 and 10.84 μm depth can be found in Section 3 of the ESI†).

The overall behaviour of the different cell types can be conveniently summarized in a two-dimensional histogram based on the outlet distributions of cells in our devices, which directly reflects their effective size. Fig. 2 shows the distributions of cells at the ends of two devices as the shear rate is varied. It is immediately apparent that the different cell types show very distinct patterns, or 'fingerprints'.

The overall plots for the shallow devices (Fig. 2A, C and E) show that the discocytes and the echinocytes have similar mechanical properties. At low shear rates it can be seen that the unperturbed sizes are comparable. As the shear rate increases the similar slopes indicate similar deformabilities. The stomatocytes show a different behaviour. First of all they have a smaller unperturbed size and a flatter slope indicating less deformability. Secondly they show a distinct bistability, something that is even more evident in the deeper device.

In the deeper devices (Fig. 2B, D and F) the projected size of the echinocyte is clearly greater than that of the discocytes. The elasticity

of the discocytes is not accessible in our deep devices since the smallest critical size is greater than half the thickness of the discocytes. On the other hand it can clearly be seen that the echinocytes have a continuous elastic deformation. The stomatocytes seem to have a more complex mechanical structure. The data show a bistable situation with a quite resilient conformation up to a relatively high shear rate at an applied pressure of about 200 mbar that quickly snaps into a different conformation.

To exclude any other driving forces beyond deformation such as hydrodynamic lift or deformation of the device itself that may be involved in decreasing R_{eff} we repeated the experiments with hard polystyrene spheres (see the ESI† Section 5) and found no systematic change in the outlet distributions over the range of shear rates used for the cells. To demonstrate the capability of our method to detect changes in deformability we fixated echinocytes using glutaraldehyde without changing their morphology. The resulting data show a decreased slope (ESI† Section 4) clearly indicating a decrease in deformability.

In conclusion, we have demonstrated a scheme for size, morphology and deformability-based manipulations using DLD that we believe will be useful for preparative and analytical separations. Size-based manipulation is inherent to DLD and we add
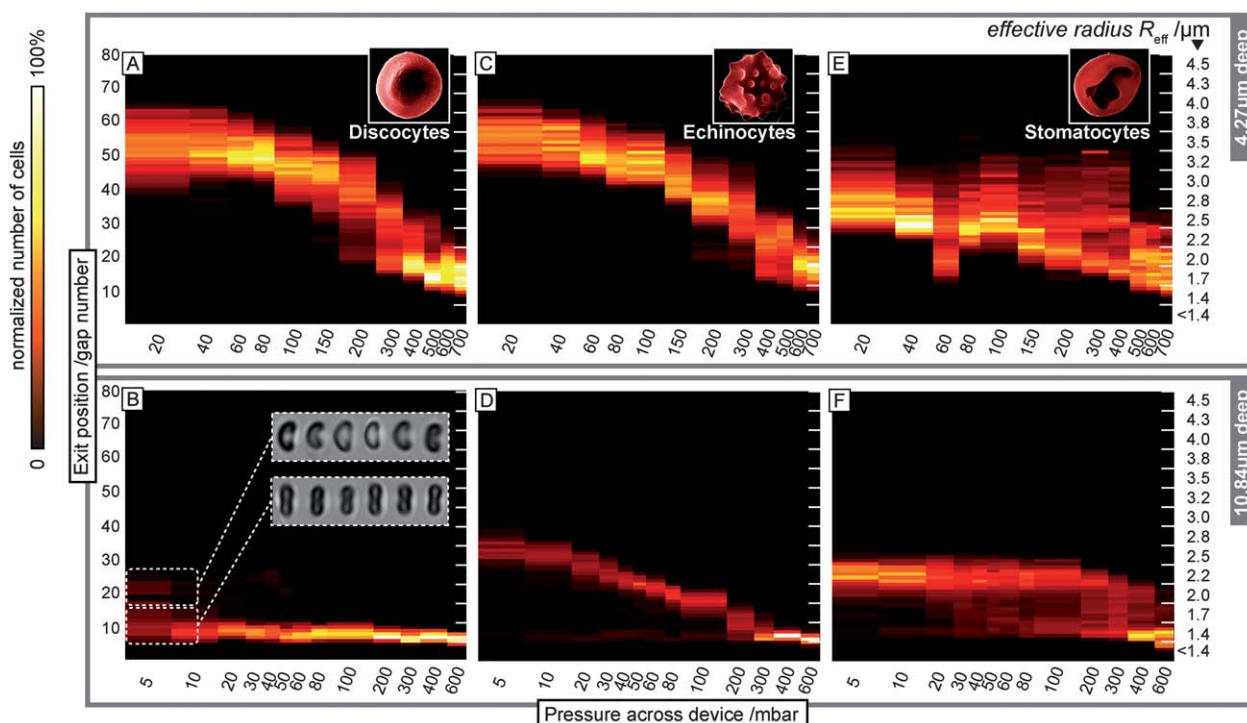

Fig. 2 The exit position (reflecting the measured effective radius, R_{eff}) as a function of applied pressure (and therefore shear rate and resulting shear stress) constitutes a cell type fingerprint. Here three red blood cell types are shown in devices of 4.27 μm depth (A, C and E) and 10.84 μm depth (B, D and F). Approximate values of the shear rates generated in our devices can be estimated by simulating fluid flow in the absence of particles. A change in driving pressure from 5 mbar to 800 mbar corresponds to average flow velocities in the range 30 μm s⁻¹ to 4.6 cm s⁻¹ and 110 μm s⁻¹ to 18 cm s⁻¹ and wall shear rates (the maximum rate at the surface of the posts) in the range 40 to 6700 s⁻¹ and 100 to 16 400 s⁻¹ for the shallow and deep devices respectively. Cells are introduced through gap 5 and so exiting the device at gap 5 constitutes no lateral displacement of the cells as they traverse the device ($R_{eff} \leq$ 1.4 μm). Increasing gap number relates to increasing R_{eff} resulting in more lateral displacement. Lateral displacement is a measure of R_{eff} and as the shear rate is increased the resulting deformation leads to a decrease in R_{eff}. Note that the different populations are not completely pure. A subpopulation of weakly stomatocytic, bowl-shaped cells is present among the discocytes as can be seen in B (we are unsure as to the exact origin of these cells but they seem to constitute a subpopulation of cells that are more susceptible to the buffer than others) and can be distinguished at low shear rates. (D) SS and (F) TX do not transform all RBCs into echinocytes and stomatocytes. For both cell types a small fraction of cells remain disc-shaped and can easily be resolved from the morphologically altered majority in the deep devices.

morphology, *via* control of particle orientation, and deformability, *via* control of shear stresses, to this simple but powerful technique. Compared to imaging cytometry (see *e.g.* Amnis and CompuCyte), our method provides a simple means to passively sort particles based on morphological characteristics with high throughput and a resolution that is not fundamentally limited by diffraction. Although constrained to fairly simple shapes we expect our technique to open up for important applications in biomedicine involving, *e.g.*, length-sorting of bacteria or yeast thereby making it possible to fractionate with respect to phase in the cell-cycle of microorganisms without the addition of any deleterious additives or treatment of the cells. Compared to existing techniques for the measurement of deformability we can provide good throughput combined with good resolution together with some information on the anisotropy of the deformability. We envision our technique to be a good candidate for extraction of, *e.g.*, circulating tumour cells from blood.

To better understand the connection between the behaviour of the cells in our device and the mechanical properties of the cellular architecture, a more detailed picture of the shear stresses experienced by cells and of those mechanical properties that affect R_{eff} need to be elucidated with the aid of, *e.g.*, full 3D simulations and artificial cell analogues. The effect of the timescales involved for deformation and mechanical relaxation is another important topic that would open up for characterization of the viscous properties of the cells. By designing the post and array geometry appropriately we could change the variation in shear rates that the cells experience. This could be used in a device to independently measure elastic and viscous properties as well as overall deformation and shape.

Acknowledgements

Notes and references

‡ These two devices are not the same as those used in the deformation measurements but have very similar dimensions.

1 S. H. Holm, J. P. Beech, M. P. Barrett and J. O. Tegenfeldt, *Lab Chip*, 2011, **11**, 1326–1332.
2 S. Sugaya, M. Yamada and M. Seki, *Biomicrofluidics*, 2011, **5**, 024103-1–024103-13.
3 M. R. Hardeman, P. T. Goedhart, J. G. G. Dobbe and K. P. Lettinga, *Clin. Hemorheol.*, 1994, **14**, 605–618.
4 J. Guck, R. Ananthakrishnan, H. Mahmood, T. J. Moon, C. C. Cunningham and J. Kas, *Biophys. J.*, 2001, **81**, 767–784.
5 J. P. Brody, Y. Q. Han, R. H. Austin and M. Bitensky, *Biophys. J.*, 1995, **68**, 2224–2232.
6 H. Bow, I. V. Pivkin, M. Diez-Silva, S. J. Goldfless, M. Dao, J. C. Niles, S. Suresh and J. Han, *Lab Chip*, 2011, **11**, 1065–1073.
7 H. W. Hou, A. A. S. Bhagat, A. G. L. Chong, P. Mao, K. S. W. Tan, J. Y. Han and C. T. Lim, *Lab Chip*, 2010, **10**, 2605–2613.
8 S. C. Hur, N. K. Henderson-MacLennan, E. R. B. McCabe and D. Di Carlo, *Lab Chip*, 2011, **11**, 912–920.
9 L. R. Huang, E. C. Cox, R. H. Austin and J. C. Sturm, *Science*, 2004, **304**, 987–990.
10 D. W. Inglis, PhD thesis: *Microfluidic Devices for Cell Separation*, Princeton University, 2007.
11 J. A. Davis, PhD Thesis: *Microfluidic Separation of Blood Components through Deterministic Lateral Displacement*, Princeton University, 2008.
12 J. A. Davis, D. W. Inglis, K. J. Morton, D. A. Lawrence, L. R. Huang, S. Y. Chou, J. C. Sturm and R. H. Austin, *Proc. Natl. Acad. Sci. U. S. A.*, 2006, **103**, 14779–14784.
13 V. Turchetti, C. De Matteis, F. Leoncini, L. Trabalzini, M. Guerrini and S. Forconi, *Clin. Hemorheol. Microcirc.*, 1997, **17**, 209–215.
14 F. C. Mokken, M. Kedaria, C. P. Henny, M. R. Hardeman and A. W. Gelb, *Ann. Hematol.*, 1992, **64**, 113–122.
15 M. P. Sheetz and S. J. Singer, *Proc. Natl. Acad. Sci. U. S. A.*, 1974, **71**, 4457–4461.
16 H. W. G. Lim, M. Wortis and R. Mukhopadhyay, *Proc. Natl. Acad. Sci. U. S. A.*, 2002, **99**, 16766–16769.
17 A. L. Li, H. Seipelt, C. Muller, Y. D. Shi and G. M. Artmann, *Pharmacol. Toxicol.*, 1999, **85**, 206–211.
18 Y. Yawata, *Cell Membrane: The Red Blood Cell as a Model*, Wiley-VCH, Weinheim, 2003.